Current Applied Physics 18 (2018) 411–416

Contents lists available at ScienceDirect

Current Applied Physics

journal homepage: www.elsevier.com/locate/cap

Unusual flow behavior of Fe-based soft magnetic amorphous ribbons under high temperature tensile loading

Jiyun Oh [a], Jin-Yoo Suh [b], Woo-Jin Kim [c], Jae-il Jang [c], Ki Hoon Kang [c], Chong Seung Yoon [c], Haein Choi-Yim [a, *]

[a] Department of Physics, Sookmyung Women's University, Seoul 04310, South Korea
[b] High Temperature Energy Materials Research Center, Korea Institute of Science and Technology, Seoul 02792, South Korea
[c] Department of Materials Science and Engineering, Hanyang University, Seoul 04763, South Korea

ARTICLE INFO

Article history:
Received 24 October 2017
Received in revised form
3 January 2018
Accepted 12 February 2018
Available online 13 February 2018

Keywords:
Fe-based amorphous alloy
Viscous flow
Nanoindentation
Soft-magnetic property

ABSTRACT

The viscous thermal flow behavior and mechanical property of $[Fe_{0.6}Co_{0.15}B_{0.2}Si_{0.05}]_{(100-x)}Ta_x$ (x = 0, 1, 2, 3, 4, and 5) soft magnetic amorphous ribbons were studied. The characteristics of melt-spun amorphous ribbons were measured by using vibration sample magnetometer (VSM), nanoindentation, differential scanning calorimetry (DSC) and thermo-mechanical analysis (TMA) to study the effects of Ta content variation on the thermal stability, mechanical, and soft magnetic properties. We observed that the nanoindentation hardness, Young's modulus, and glass transition and crystallization temperatures were improved by the addition of Ta. Using dilatometry measurement, TMA, by heating at a constant rate under tension mode, we examined not only the glass transition and crystallization behaviors but also the possibility of coexistence of multiple amorphous phases.

1. Introduction

The synthesis of an Fe-based amorphous alloy was first conducted with the Fe-P-C system in 1967 by Paul Duwez's group [1], and Fe-based bulk metallic glasses (BMGs), of the Fe-Al-Ga-P-C-B alloy system, were first synthesized in 1995 by Inoue et al. [2]. Thereafter, research on Fe-based amorphous alloys has been consistently pursued [3–8]. Fe-based amorphous alloys are well known for their excellent soft magnetic properties, such as high saturation magnetization (M_s) and low coercivity (H_c), as well as other promising engineering properties including physical, mechanical, and corrosion-resistance properties [9–11].

Among the Fe-based amorphous alloys, the Fe-Co-B-Si alloy system was reported to demonstrate promising soft magnetic properties [12–15]. Additionally, the substitution of Fe with Co turned out to be an effective method to enhance the M_s value of the amorphous metallic structure [16]. In tailoring the properties of interest, the addition of minor alloying elements and optimization of their concentrations are key processes in alloy development. The effect of a refractory element, Ta, on the magnetic and other properties of Fe-based amorphous alloys has rarely been reported [3,17]; systematic study on the effect of Ta concentration was little carried out in Refs. [3,17]. Therefore, the major effect of Ta concentration variation on the physical properties of Fe-based amorphous alloys including magnetic, mechanical, and thermomechanical properties needs to be clarified. Ta has a high density, high elastic modulus, and high melting point, and thus, the Ta is mainly used as a minor alloying element for improving various properties of alloys [18]. Therefore, in this study, we added Ta to the Fe-Co-B-Si alloy system and reported the effect of Ta addition and its variation in concentration on the mechanical and viscous flow behaviors.

In the development and characterization of Fe-based amorphous alloys, defining the glass transition temperature (T_g) is one of the most tricky tasks, probably owing to the limited glass-forming ability of the alloys, which is generally measured using differential scanning calorimetry (DSC) at a constant heating rate. The glass transition taking place during the heating of an amorphous structure is a transition from a structurally frozen state to a super-cooled liquid state, which is accompanied by an increase in heat capacity resulting in a slight deflection of the DSC baseline toward the direction of heat absorption. However, for most Fe-based amorphous alloys investigated for their soft magnetic properties, the DSC baselines do not show a sufficiently clear deflection to define the T_g.

* Corresponding author.
E-mail address: haein@sm.ac.kr (H. Choi-Yim).

https://doi.org/10.1016/j.cap.2018.02.005
1567-1739/

To date, the unclear T_g has been tentatively attributed to the limited glass-forming ability of the alloys, and no further studies have been performed in this regard. Additionally, the thermal behaviors of Fe-based amorphous alloys have been less thoroughly investigated than those of other alloys such as Cu-, Mg-, and Zr-based alloys [19–23].

In our previous work, we focused on the magnetic properties of the Fe-Co-B-Si-Ta amorphous alloy system with focusing on the variation of Fe/Co concentration ratio utilizing the positive effect of Ta addition by fixing its concentration [24,25]. Here, we focused on the thermal analysis of the amorphous phases and mechanical properties of the Fe-Co-B-Si-Ta amorphous alloy system. Moreover, we performed a different thermal analysis, utilizing dilatometry measurements of thin ribbons under tension mode to define the glass transition behavior of Fe-based amorphous alloys with varying chemical compositions. It turned out that the dilatometry measurement of amorphous ribbons not only enabled the successful evaluation of the glass transition and crystallization behavior, but also suggested the possibility of coexistence of multiple amorphous phases. Therefore, in this study, we reported the unusual viscous flow behavior of Fe-based amorphous alloy ribbons with varying Ta content and discussed the measured thermal stability of the amorphous phases and other properties.

2. Experiments

Multi-component alloys with nominal atomic percentage compositions of $[Fe_{0.6}Co_{0.15}B_{0.2}Si_{0.05}]_{(100-x)}Ta_x$ (x = 0, 1, 2, 3, 4, and 5) were prepared by arc-melting under a Ti-gettered argon atmosphere. The alloys were prepared by using high-purity metals of Fe (99.95%), Co (99.95%), B (99.5%), Si (99.999%), and Ta (99.95%). To minimize the chemical inhomogeneity, we remelted the alloy ingots at least six times. Amorphous alloy ribbons were rapidly solidified by melt-spinning method under an argon atmosphere with a copper wheel speed of 45.81 m/s. The as-spun amorphous ribbons had a thickness and width of approximately 30 μm and 2–2.5 mm, respectively.

The amorphous structure of the as-spun ribbons was confirmed by X-ray diffraction (XRD) with Cu-Kα radiation. The saturation magnetization, M_s, was measured by vibration sample magnetometer (VSM) under in-plane applied magnetic fields in the range from −1.0 to 1.0 T. The nanoindentation hardness (H_N) and Young's modulus (E) were examined by a nanoindentation tester (MTS Nanoindenter XP) with a pyramidal Berkovich diamond tip using a continuous stiffness measurement (CSM) technique at a controlled frequency 45 Hz. In CSM mode, the contact stiffness is continuously measured while the nanoindenter is loading at a regular frequency [26]. The nanoindentation was performed with a maximum load of 50 mN at constant loading/unloading rates of 1.67 mN/s and the indenter was held at the maximum load for 1 s. We also assigned a Poisson's ratio of 0.3. Each indentation test was repeated 20 times under the same experimental conditions to increase accuracy of the data and the average values of 20 separate measurements were used. The ribbon samples were mechanically polished down to 0.05 μm colloidal silica suspension to obtain a mirror-like appearance. After the nanoindentation experiment, the surface profile was examined by atomic force microscopy (AFM) and we applied a Pt-coating to the surface with indented regions to prepare for scanning electron microscopy (SEM) observations. Then, the appearance of each indentation was examined by SEM.

The crystallization temperature ($T_{x,\ DSC}$) was measured by DSC curves under an argon atmosphere at a heating rate of 0.34 K/s. Amorphous samples with an approximate mass of 20–30 mg were used for the DSC measurements. The viscous flow behavior of the super-cooled liquid region, temperature dependence of the relative displacement, T_g, and crystallization temperature ($T_{x,\ TMA}$) were measured by thermomechanical analysis (TMA) using the thermomechanical analyzer device under a tensile loading mode. The as-spun ribbons were directly cut by using scissors to be installed in the sample holder of the TMA apparatus with a gauge length of 10 mm (shown in Fig. 8(a)). The applied load and heating rate were 700 mN and 0.17 K/s, respectively.

3. Results and discussion

The chemical composition with the nominal atomic percentage of the Fe-Co-B-Si-Ta alloy system is given in Table 1. Fig. 1 shows the XRD patterns of the $[Fe_{0.6}Co_{0.15}B_{0.2}Si_{0.05}]_{(100-x)}Ta_x$ (x = 0, 1, 2, 3, 4, and 5) melt-spun ribbons. The XRD patterns show only broad halo humps without any crystalline peaks, which indicates the non-periodic atomic arrangement of an amorphous phase.

The intrinsic magnetic property of the Fe-Co-B-Si-Ta melt-spun ribbon was studied by using VSM. Fig. 2(a) shows hysteresis M-H loops of the melt-spun ribbons; Fig. 2(b) shows the dependency of M_s on the Ta content and the obtained values of M_s are also listed in Table 2. It is obvious from the hysteresis M-H loops that all the amorphous ribbons have soft magnetic characteristics. The highest and lowest values of M_s were 149.6 and 101.2 emu/g for the $Fe_{60}Co_{15}B_{20}Si_5$ (x = 0) and $Fe_{57}Co_{14.25}B_{19}Si_{4.75}Ta_5$ (x = 5) ribbons, respectively. As the Ta content increased from 0 to 5 at.%, M_s decreased from 149.6 to 101.2 emu/g. This significant drop in M_s appeared to be more than that expected owing to the change in Fe content from 60 to 57 at.% (with Ta contents ranging from 0 to 5 at.%). Although this is difficult to explain, the unusual behavior might suggest the existence of multiple amorphous phases and the variation of the relative phase fractions as a function of Ta concentration, for example, a Fe-rich clustering contributing to high M_s value that could exist in the amorphous structure could have been suppressed by the addition of Ta. No direct proof has been provided yet, but indirect evidences are reported in the following sections. Nevertheless, further study seeking the direct evidence for the discussion given above should be conducted.

The mechanical properties such as hardness and modulus are shown in Fig. 3(a) and (b). Typical load–displacement (p–h) curves of the Fe-Co-B-Si-Ta melt-spun ribbons are shown in Fig. 3(a) except for the thermal drift section. With the increase in Ta content, the maximum indentation depth decreased from 1086.16 to 535.11 nm, which indicates that the hardness is significantly influenced by the Ta content. Additionally, it was confirmed that the addition of Ta induces mechanical hardening of the ribbons. H_N and E are presented in Fig. 3(b) with error bars, which indicate the scattering of the values acquired by 20 repeated indentations. As shown in Fig. 3(b), the H_N and E values consistently increase with increasing Ta content, and the average values of H_N and E are listed in Table 2. The maximum values of H_N and E are 11.90 and 112.31 GPa, respectively, for the $Fe_{57}Co_{14.25}B_{19}Si_{4.75}Ta_5$ (x = 5) alloy. The H_N values range from 5.44 to 11.90 GPa and the E values range from 21.66 to 112.31 GPa. It should be noted here that Ta addition to a level of 5 at.% induced a two-fold increase in H_N and a five-fold

Table 1
Chemical composition of Fe-Co-B-Si-Ta amorphous alloys (at.%).

$[Fe_{0.6}\ Co_{0.15}\ B_{0.2}\ Si_{0.05}]_{(100-x)}Ta_x$	Fe	Co	B	Si	Ta
x = 0	60	15	20	5	0
x = 1	59.4	14.85	19.8	4.95	1
x = 2	58.8	14.7	19.6	4.9	2
x = 3	58.2	14.55	19.4	4.85	3
x = 4	57.6	14.4	19.2	4.8	4
x = 5	57	14.25	19	4.75	5

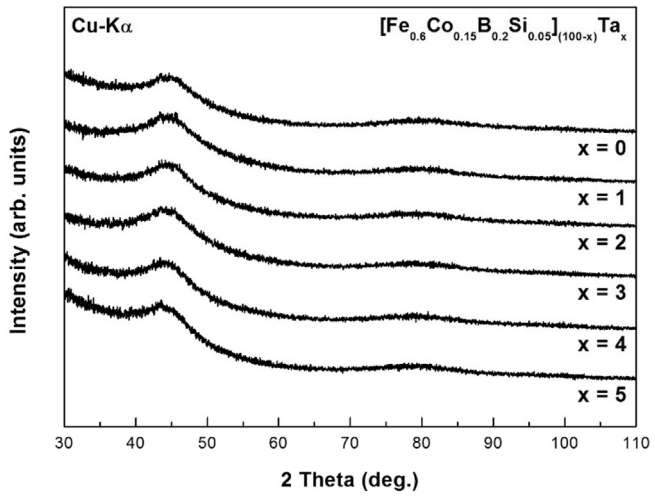

Fig. 1. X-ray diffraction patterns of melt-spun ribbons.

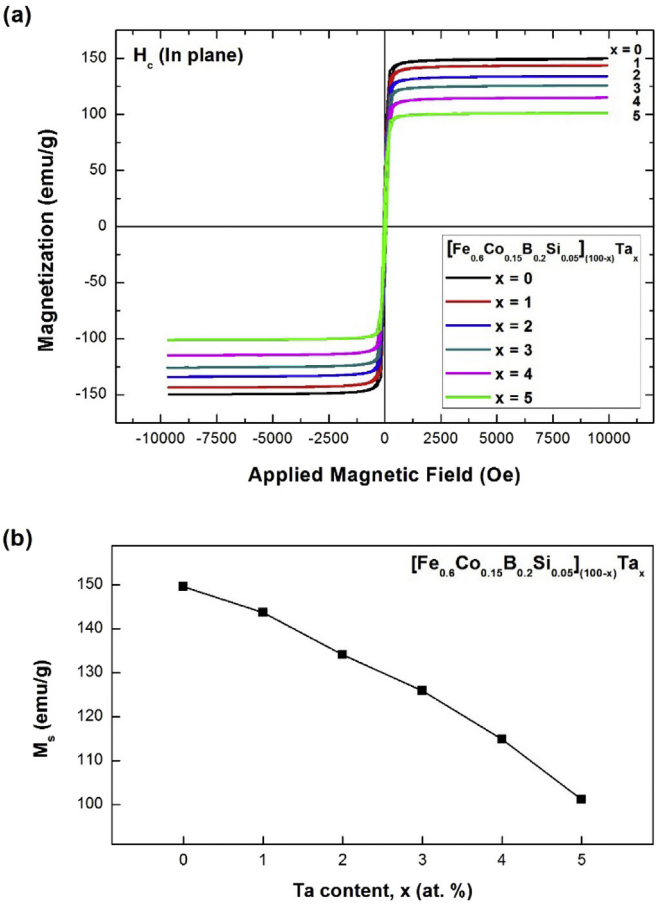

Fig. 2. (a) Hysteresis loops and (b) saturation magnetizations (M_s) of $[Fe_{0.6}Co_{0.15}B_{0.2}Si_{0.05}]_{(100-x)}Ta_x$ (x = 0, 1, 2, 3, 4, and 5) melt-spun ribbons.

increase in E. Similar to the drastic change in the magnetic property induced by 5 at.% Ta addition (shown in Fig. 2(b)), the changes in the mechanical and physical properties appear quite significant, considering the minor changes in chemical composition. This abrupt change in mechanical and elastic properties that is more than that expected simply from the minor change in chemical composition also suggests the possible formation of

Table 2
Magnetic property (M_s) and mechanical properties (average values of H_N and E) of $[Fe_{0.6}Co_{0.15}B_{0.2}Si_{0.05}]_{(100-x)}Ta_x$ (x = 0, 1, 2, 3, 4, and 5) melt-spun ribbons.

x	Alloys	Magnetic Property	Mechanical Properties	
		M_s (emu/g)	H_N (GPa)	E (GPa)
0	$Fe_{60}Co_{15}B_{20}Si_5$	149.6	5.44	21.66
1	$Fe_{59.4}Co_{14.85}B_{19.8}Si_{4.95}Ta_1$	143.7	7.60	47.53
2	$Fe_{58.8}Co_{14.7}B_{19.6}Si_{4.9}Ta_2$	134.1	7.70	39.08
3	$Fe_{58.2}Co_{14.55}B_{19.4}Si_{4.85}Ta_3$	125.9	9.37	54.41
4	$Fe_{57.6}Co_{14.4}B_{19.2}Si_{4.8}Ta_4$	114.9	10.27	68.53
5	$Fe_{57}Co_{14.25}B_{19}Si_{4.75}Ta_5$	101.2	11.90	112.31

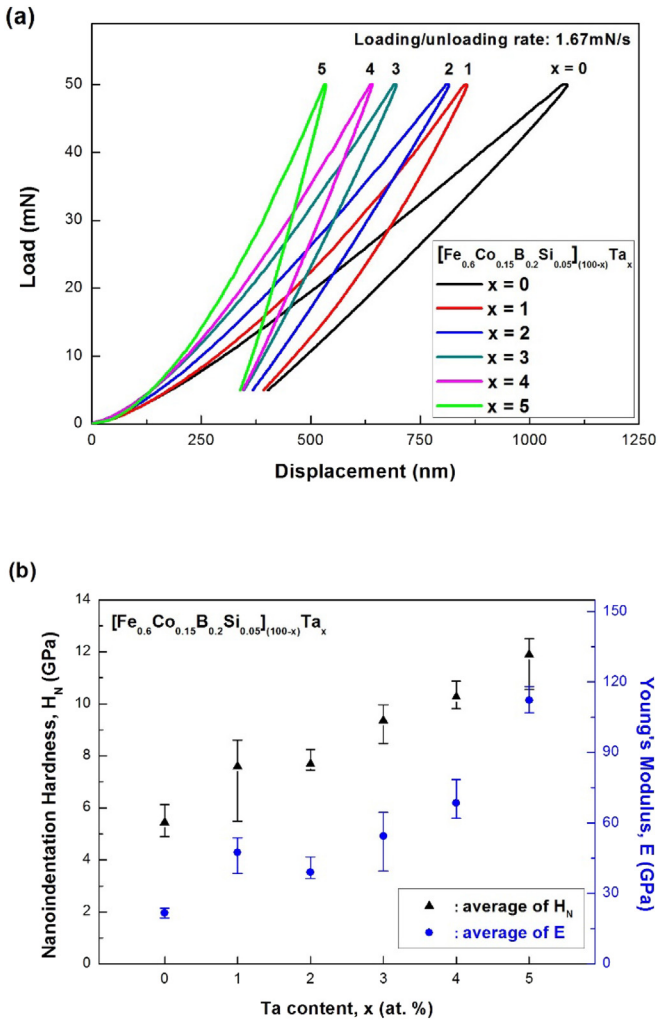

Fig. 3. (a) Load–displacement (p–h) curves and (b) nanoindentation hardness (H_N) and Young's modulus (E) of the $[Fe_{0.6}Co_{0.15}B_{0.2}Si_{0.05}]_{(100-x)}Ta_x$ (x = 0, 1, 2, 3, 4, and 5) melt-spun ribbons.

inhomogeneous amorphous structure; soft and less-stiff Fe-rich clustering might have been suppressed by the increase in Ta concentration.

Fig. 4 exhibits the localized indentation behavior observed by SEM and AFM. Fig. 4(a) shows the cross profiles of an indent that marks on the surfaces of the two alloys, $[Fe_{0.6}Co_{0.15}B_{0.2}Si_{0.05}]_{(100-x)}Ta_x$ (x = 0, 5), and the pile-up around the indents were confirmed by AFM. The cross profiles were measured in the direction of the dotted line of the indent photograph and the

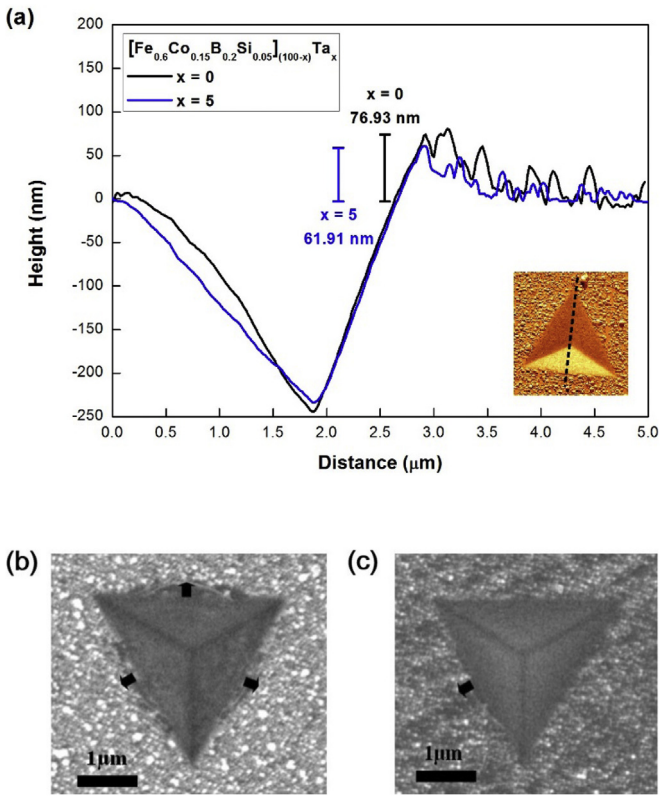

Fig. 4. (a) Surface profile of the samples observed by AFM and appearance of indents observed by SEM for the alloys of (b) $Fe_{60}Co_{15}B_{20}Si_5$ (x = 0, left) and (c) $Fe_{57}Co_{14.25}B_{19}Si_{4.75}Ta_5$ (x = 5, right).

markedlines of the pile-up values shown in Fig. 4(a). The pile-up around the indent is 76.93 nm for the $Fe_{60}Co_{15}B_{20}Si_5$ (x = 0) ribbon, which has the lowest H_N value, and 61.91 nm for the $Fe_{57}Co_{14.25}B_{19}Si_{4.75}Ta_5$ (x = 5), ribbon which has the highest H_N value. These data indicate that the higher the pile-up, the more mechanically soft is the alloy. Therefore, the AFM profile shows the relation between the pile-up height and hardness. After the AFM experiment, the indented regions were observed by SEM. Fig. 4(b) and (c) show the shear band appearance around the indents, which are marked by the arrows. The semicircular shear bands observed around the indents are due to the plastic deformation of the sample. More shear bands were observed for the mechanically soft $Fe_{60}Co_{15}B_{20}Si_5$ (x = 0) ribbon (shown in Fig. 4(b)). In the harder $Fe_{57}Co_{14.25}B_{19}Si_{4.75}Ta_5$ (x = 5) ribbon, the shear band was hardly visible (shown in Fig. 4(c)). The more obvious shear band appearance corresponds to lower hardness.

To evaluate the thermal properties of the Fe-Co-B-Si-Ta alloy ribbons, we conducted DSC and TMA experiments under an argon atmosphere and observed the unusual thermal behavior of the alloys. Fig. 5 shows DSC curves of the melt-spun $[Fe_{0.6}Co_{0.15}B_{0.2}Si_{0.05}]_{(100-x)}Ta_x$ (x = 0, 1, 2, 3, 4, and 5) ribbons. We identified the crystallization peaks and the primary $T_{x,\ DSC}$, which were measured by DSC, and the primary $T_{x,\ DSC}$ values are marked by arrows in the DSC curves. With the increase in Ta content from 0 to 5 at.%, the $T_{x,\ DSC}$ increased from 822.3 to 875.2 K (given in Table 3) and the highest value was acquired for the alloy $Fe_{57}Co_{14.25}B_{19}Si_{4.75}Ta_5$ (x = 5). It may be assumed that the $Fe_{57}Co_{14.25}B_{19}Si_{4.75}Ta_5$ (x = 5) amorphous alloy ribbon with high $T_{x,\ DSC}$ is structurally stable. We observed that all the DSC traces have several distinct crystallization exothermic peaks. Therefore, we could judge that all melt-spun ribbons had at least two amorphous phases. In the DSC traces, a

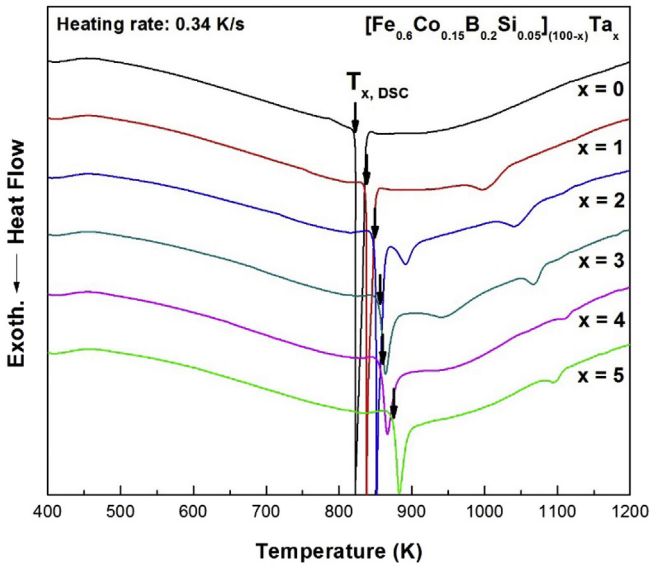

Fig. 5. DSC curves of $[Fe_{0.6}Co_{0.15}B_{0.2}Si_{0.05}]_{(100-x)}Ta_x$ (x = 0, 1, 2, 3, 4, and 5) melt-spun ribbons.

Table 3
Thermal properties such as T_g, $T_{x,\ TMA}$, $T_{x,\ DSC}$, and ΔT_x of the $[Fe_{0.6}Co_{0.15}B_{0.2}Si_{0.05}]_{(100-x)}Ta_x$ (x = 0, 1, 2, 3, 4, and 5) melt-spun ribbons.

x	Alloys	Thermal Properties (K)			
		T_g	$T_{x,\ TMA}$	$T_{x,\ DSC}$	ΔT_x ($= T_{x,\ TMA} - T_g$)
0	$Fe_{60}Co_{15}B_{20}Si_5$	734.8	756.1	822.3	21.3
1	$Fe_{59.4}Co_{14.85}B_{19.8}Si_{4.95}Ta_1$	754.2	770.3	837.9	16.1
2	$Fe_{58.8}Co_{14.7}B_{19.6}Si_{4.9}Ta_2$	763.6	784.3	849.5	20.7
3	$Fe_{58.2}Co_{14.55}B_{19.4}Si_{4.85}Ta_3$	765.5	779.4	856.6	13.9
4	$Fe_{57.6}Co_{14.4}B_{19.2}Si_{4.8}Ta_4$	768.3	785.8	860.1	17.5
5	$Fe_{57}Co_{14.25}B_{19}Si_{4.75}Ta_5$	779.7	801.2	875.2	21.5

clear T_g value could not be obtained from all ribbons, because the high Fe content in Fe-based alloys caused the low tendency of amorphous structure formation [5].

TMA is an efficient technique to identify the T_g values, and thus, we can determine T_g as the starting point of the super-cooled liquid region, that is the onset point of the elongation in the displacement–temperature plot (shown in Fig. 6). Additionally, we

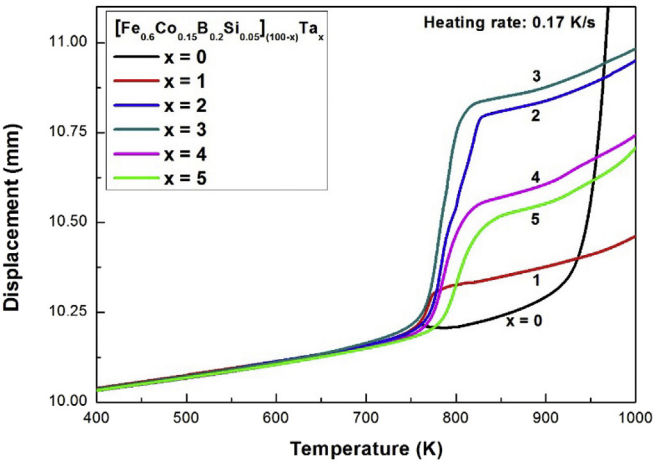

Fig. 6. Temperature dependence of the displacement for the $[Fe_{0.6}Co_{0.15}B_{0.2}Si_{0.05}]_{(100-x)}Ta_x$ (x = 0, 1, 2, 3, 4, and 5) melt-spun ribbons.

studied the change in viscous flow (viscosity) of the melt-spun alloys during nonisothermal tensile loading tests. The temperature dependence of the ribbon length under heating at a constant rate of 0.17 K/s is indicated in Fig. 6. It is noted in Fig. 6 that the $Fe_{60}Co_{15}B_{20}Si_5$ (x = 0) melt-spun ribbon shows a small elongation around the first crystallization (around 750 K) and then very large elongation at temperatures higher than 900 K. The slight bump around 750 K, consisting of a slight increase (glass transition) in displacement followed by a contraction (crystallization), and the large elongation after 900 K indicate that the first crystallization peak shown in the DSC curve (shown in Fig. 5) could be the crystallization of only a small fraction of the entire amorphous metal. In other words, the major fraction of the metal still remains as amorphous even after the first crystallization peak and contributes to the massive flow behavior above 900 K. The viscous flow was so active that the specimen failed in the middle of the heating process prior to the crystallization of the flowing super-cooled liquid phase (shown in Fig. 8(b)). However, the alloys with Ta addition showed different flow behavior; the ribbons containing Ta showed enhanced flow behavior for their first glass transition and did not show as much of the low temperature flow behavior as the alloy $Fe_{60}Co_{15}B_{20}Si_5$ (x = 0). The Ta-added ribbons showed similar elongation behavior, and among them, the $Fe_{58.2}Co_{14.55}B_{19.4}Si_{4.85}Ta_3$ (x = 3) melt-spun ribbon showed the largest elongation.

Fig. 7(a) and (b) show the calculated viscosity of the melt-spun ribbons using the relation $\eta = \sigma/3\dot{\varepsilon}$ [27], where η is the viscosity, σ is the applied tensile stress, and $\dot{\varepsilon}$ is the tensile strain rate. In Fig. 7(a), the viscosities of different alloys are expressed together in the same plot, and in Fig. 7(b), the viscosity curves are separated for clarity. The T_g value obtained from Fig. 6 is marked by the arrows in Fig. 7(b). The viscosity values of the melt-spun ribbons are in the range 10^{10}–10^{12} Pa s. As the temperature increases beyond T_g, the viscosity begins to decrease consistently to the lowest value of ~10^{10} Pa s. At a certain temperature during the super-cooled liquid flow, crystallization starts to occur and then viscosity increases again. With the increase in Ta content from 0 to 5 at.%, the T_g value increases from 734.8 to 779.7 K, as observed in Table 3, and the highest value is acquired for the alloy $Fe_{57}Co_{14.25}B_{19}Si_{4.75}Ta_5$ (x = 5). The primary crystallization temperature value, which is measured by TMA, $T_{x,\ TMA}$, generally increases with the Ta content, except for $Fe_{58.2}Co_{14.55}B_{19.4}Si_{4.85}Ta_3$ (x = 3). The primary $T_{x,\ TMA}$ is determined from the minimum point of the viscosity curves and the values are marked by the arrows in Fig. 7(b). ΔT_x (= $T_{x,\ TMA} - T_g$) is the highest for $Fe_{57}Co_{14.25}B_{19}Si_{4.75}Ta_5$ (x = 5), and therefore we can estimate that the x = 5 melt-spun ribbon is the most thermally stable of all the ribbons. The thermal characteristics, such as T_g, $T_{x,\ TMA}$, $T_{x,\ DSC}$, and ΔT_x of all the ribbons are listed in Table 3.

In viscous flow, we determined that the primary crystallization is not indicative of the whole phase transition of the amorphous ribbons. As in the DSC curves, various amorphous phases were also detected in the viscosity curves (shown in Fig. 7(a) and (b)). In the $Fe_{60}Co_{15}B_{20}Si_5$ (x = 0) ribbon, the second glass transition showed a larger viscosity decrease than the first glass transition as in the TMA viscosity flows. The larger viscosity decrease occurred at a high temperature, which means that the proportion of the high temperature amorphous phase must be dominant. This is in contrast to the $Fe_{60}Co_{15}B_{20}Si_5$ (x = 0) ribbon, to which when Ta is added, the viscosity decrease in the first crystallization is large, and thus, the proportion of the low temperature amorphous phase is large. Therefore, when Ta is added to the Fe-based alloy, the amounts of the low and high temperature amorphous phases switch. Additionally, as shown in Figs. 5 and 7, we can identify that as more Ta is added to the Fe-based alloy, the crystallization reaction shifts to higher temperature. It should be noted that, as the content of Ta increases, the phase change kinetics slow down. Fig. 8 shows the

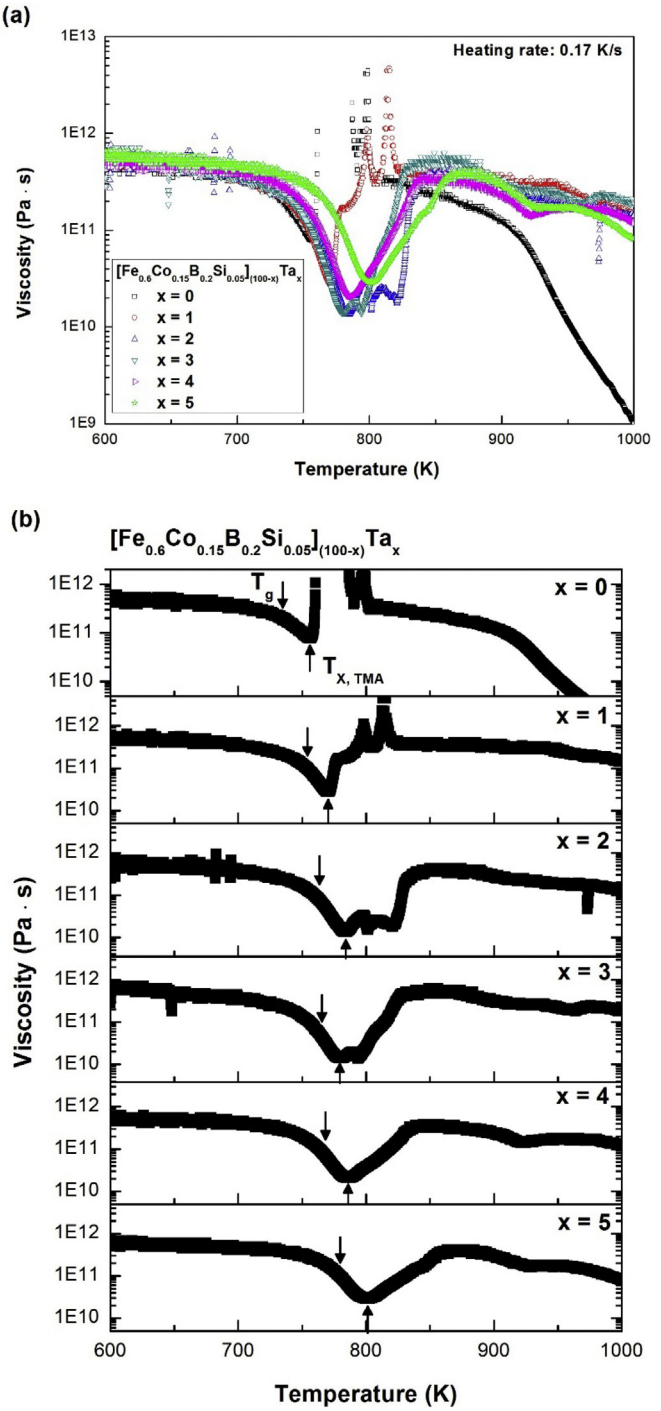

Fig. 7. (a), (b) Temperature dependence of the effective viscosity for the $[Fe_{0.6}Co_{0.15}B_{0.2}Si_{0.05}]_{(100-x)}Ta_x$ (x = 0, 1, 2, 3, 4, and 5) melt-spun ribbons.

elongation of a melt-spun ribbon sample after the TMA tensile mode experiment. Fig. 8(a) and (b) are the photographs of the $Fe_{60}Co_{15}B_{20}Si_5$ (x = 0) ribbon installed in the TMA tensile fixture before and after experiment, respectively.

We observed the unusually significant change in the magnetic (shown in Fig. 2(b)), physical, and mechanical properties (shown in Fig. 3(b)) induced by the minor compositional variation of only 5 at.% Ta addition. By the thermal analyses utilizing two different methods, DSC and TMA, it was also found that the $Fe_{60}Co_{15}B_{20}Si_5$ (x = 0) alloy is composed of multiple amorphous phases with

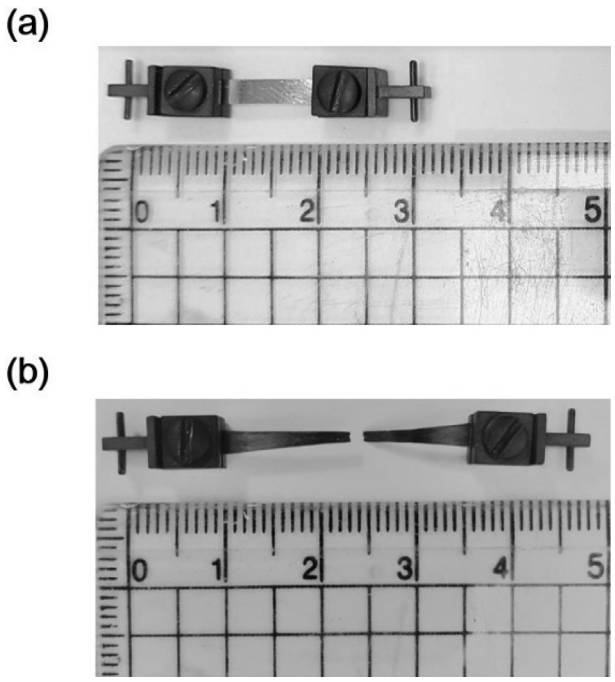

Fig. 8. Photographs of $Fe_{60}Co_{15}B_{20}Si_5$ (x = 0) melt-spun ribbon with TMA tensile probe (a) before experiment and (b) after experiment.

different chemical compositions. Moreover, the Ta addition appears to dominantly modify the relative phase fractions such that only 1 at.% of Ta induced a significant change in the viscous flow behavior (shown in Fig. 7(b)). Therefore, it could be claimed that (i) the Fe-Co-B-Si amorphous metallic system is composed of multiple amorphous phases with different chemical compositions and (ii) adding a small amount of Ta induced a significant change in the phase fraction, resulting in a drastic change in the physical, mechanical, and magnetic properties. In this context, it is very important to acquire thorough information on the thermal, magnetic, physical, and mechanical properties of Fe-based amorphous alloys for the development of novel alloys with optimum magnetic and other engineering properties.

4. Conclusion

The mechanical and magnetic characteristics as well as the unusual flow behavior of super-cooled liquid region of the $[Fe_{0.6}Co_{0.15}B_{0.2}Si_{0.05}]_{(100-x)}Ta_x$ (x = 0, 1, 2, 3, 4, and 5) amorphous ribbons were studied in this work. Various features of the Fe-Co-B-Si-Ta system were measured by VSM, nanoindentation, DSC, and TMA.

Melt-spun ribbons showed typical soft magnetic hysteresis M–H loops. Despite a 3 at.% reduction in Fe content, the M_s value decreased drastically. Therefore, we could surmise that the existence of multiple amorphous phases and the variation in Ta content contribute to the decreasing tendency of the magnetic property. As the Ta content increases, the H_N and E values increase. As the addition of Ta increased to 5 at.%, the H_N and E values increased by factors of two and five, respectively. Therefore, we could estimate that the addition of Ta induces improvements in the mechanical properties of amorphous alloys.

By thermal analyses using two different methods, DSC and TMA, we determined that the primary crystallization is not indicative of the whole phase transition of the amorphous alloys, and that multiple amorphous phases may coexist in amorphous alloys. Additionally, Ta addition plays an important role in adjusting the relative phase fractions such that only 1 at.% of Ta induced a significant change in the viscous flow behavior.

In this paper, we discussed the effects of Ta content on the thermal, magnetic, physical, and mechanical properties of Fe-based amorphous alloys and the unusual behavior of the thermal viscous flow. Therefore, we can predict the feasibility of analogous novel studies on magnetic, thermal and other engineering properties.

Acknowledgements

This work was supported by the National Research Foundation of Korea (NRF) funded by the Ministry of Science, ICT and Future Planning (MSIP) (2015005294) and the Commercializations Promotion Agency for R&D Outcomes (COMPA) funded by the MSIP (2017K000476).

References

[1] P. Duwez, S.C.H. Lin, J. Appl. Phys. 38 (1967) 4096–4097.
[2] A. Inoue, Y. Shinohara, J.S. Gook, Mater. Trans. JIM 36 (1995) 1427–1433.
[3] H. Koshiba, A. Inoue, A. Makino, J. Appl. Phys. 85 (1999) 5136–5138.
[4] K. Yubuta, E. Mund, A. Makino, A. Inoue, Mater. Trans. 49 (2008) 1780–1784.
[5] H.R. Lashgari, Z. Chen, X.Z. Liao, D. Chu, M. Ferry, S. Li, Mater. Sci. Eng. A 626 (2015) 480–499.
[6] Y. Han, F.L. Kong, F.F. Han, A. Inoue, S.L. Zhu, E. Shalaan, F. Al-Marzouki, Intermetallics 76 (2016) 18–25.
[7] B. Han, Y.K. Kim, H. Choi-Yim, Cur. Appl. Phys. 14 (2014) 685–687.
[8] S. Kim, B. Han, J. Suh, S. Kim, D. Kim, Y.K. Kim, H. Choi-Yim, 90 (2017) 164–168.
[9] T. Egami, Rep. Prog. Phys. 47 (1984) 1601–1725.
[10] A. Inoue, B.L. Shen, C.T. Chang, Intermetallics 14 (2006) 936–944.
[11] A. Inoue, Mater. Sci. Eng. A 304–306 (2001) 1–10.
[12] H.H. Liebermann, Rapidly Solidified Alloys, first ed., Marcel Dekker Inc., New York, 1993.
[13] I.C. Rho, C.S. Yoon, C.K. Kim, T.Y. Byun, K.S. Hong, J. Non Cryst. Solids 316 (2003) 289–296.
[14] F. Wang, A. Inoue, Y. Han, F.L. Kong, S.L. Zhu, E. Shalaan, F. Al-Marzouki, A. Obaid, J. Alloys Compd. 711 (2017) 132–142.
[15] F. Wang, A. Inoue, Y. Han, S.L. Zhu, F.L. Kong, E. Zanaeva, G.D. Liu, E. Shalaan, F. Al-Marzouki, A. Obaid, J. Alloys Compd. 723 (2017) 376–384.
[16] B. Shen, A. Inoue, C. Chang, Appl. Phys. Lett. 85 (2004) 4911–4913.
[17] X.C. Zhong, H.C. Tian, S.S. Wang, Z.W. Liu, Z.G. Zheng, D.C. Zeng, J. Alloys Compd. 633 (2015) 188–193.
[18] D. Meng, J. Yi, D.Q. Zhao, D.W. Ding, H.Y. Bai, M.X. Pan, W.H. Wang, J. Non Cryst. Solids 357 (2011) 1787–1790.
[19] S.V. Ketov, A. Inoue, H. Kato, D.V. Louzguine-Luzgin, Scr. Mater. 68 (2013) 219–222.
[20] Y.C. Chang, T.H. Hung, H.M. Chen, J.C. Huang, T.G. Nieh, C.J. Lee, Intermetallics 15 (2007) 1303–1308.
[21] W. Myung, S. Ryu, I. Hwang, H. Kim, T. Zhang, A. Inoue, A.L. Greer, Mater. Sci. Eng. A 304–306 (2001) 691–695.
[22] A. Inoue, Y. Kawamura, T. Shibata, K. Sasamori, Mater. Trans. JIM 37 (1996) 1337–1341.
[23] W. Myung, K. Park, D. Jang, L. Battezzati, T. Zhang, A. Inoue, T. Masumoto, Mater. Sci. Eng. A 226–228 (1997) 406–409.
[24] H. Jo, B. Han, H. Choi-Yim, W. Kwon, J. Kor. Phys. Soc. 62 (2013) 523–526.
[25] J. Oh, H. Choi-Yim, K.H. Kang, J. Kor. Phys. Soc. 69 (2016) 1813–1816.
[26] W.C. Oliver, G.M. Pharr, J. Mater. Res. 19 (2004) 3–20.
[27] W.F. Hosford, Mechanical Behavior of Materials, first ed., Cambridge University Press, New York, 2005.